JACS
JOURNAL OF THE AMERICAN CHEMICAL SOCIETY

Article

pubs.acs.org/JACS

A Sacrificial Coating Strategy Toward Enhancement of Metal–Support Interaction for Ultrastable Au Nanocatalysts

Wangcheng Zhan,[†,‡] Qian He,[§] Xiaofei Liu,[†,‡] Yanglong Guo,[†] Yanqin Wang,[†] Li Wang,[†,‡] Yun Guo,[†] Albina Y. Borisevich,[§] Jinshui Zhang,*[,‡] Guanzhong Lu,[†] and Sheng Dai*[,‡,∥]

[†]Key Laboratory for Advanced Materials and Research Institute of Industrial Catalysis, East China University of Science and Technology, 130 Meilong Road, Shanghai 200237, PR China

[‡]Chemical Sciences Division and [§]Materials Science and Technology Division, Oak Ridge National Laboratory, Oak Ridge, Tennessee 37831, United States

[∥]Department of Chemistry, University of Tennessee, Knoxville, Tennessee 37996, United States

Supporting Information

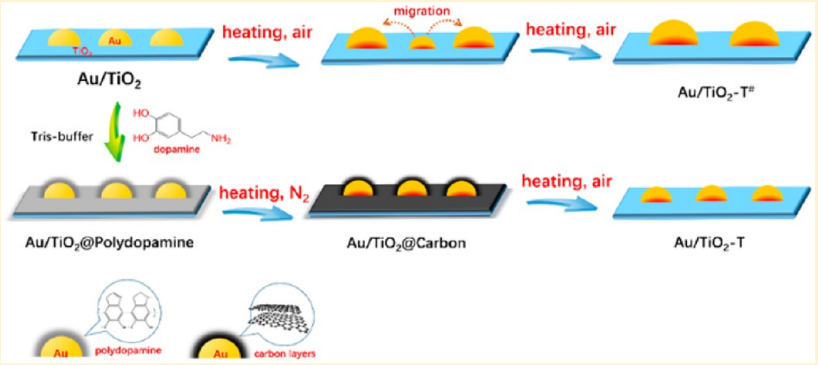

ABSTRACT: Supported gold (Au) nanocatalysts hold great promise for heterogeneous catalysis; however, their practical application is greatly hampered by poor thermodynamic stability. Herein, a general synthetic strategy is reported where discrete metal nanoparticles are made resistant to sintering, preserving their catalytic activities in high-temperature oxidation processes. Taking advantage of the unique coating chemistry of dopamine, sacrificial carbon layers are constructed on the material surface, stabilizing the supported catalyst. Upon annealing at high temperature under an inert atmosphere, the interactions between support and metal nanoparticle are dramatically enhanced, while the sacrificial carbon layers can be subsequently removed through oxidative calcination in air. Owing to the improved metal–support contact and strengthened electronic interactions, the resulting Au nanocatalysts are resistant to sintering and exhibit excellent durability for catalytic combustion of propylene at elevated temperatures. Moreover, the facile synthetic strategy can be extended to the stabilization of other supported catalysts on a broad range of supports, providing a general approach to enhancing the thermal stability and sintering resistance of supported nanocatalysts.

INTRODUCTION

Supported gold (Au) nanocatalysts are attracting increasing attention because of their unique catalytic performance for a broad range of important chemical reactions, including oxidation of CO and hydrocarbons, the water–gas shift reaction, and selective hydrogenation.[1−10] It is generally acknowledged that the catalytic properties of supported Au nanocatalysts, such as activity, selectivity, and stability, are markedly dependent on the particle size of the Au, the nature of the support, and the metal–support interaction.[11−17] The manipulation of these parameters to tune the catalytic performance therefore is of great importance to the application of Au nanocatalysts.[4,5] However, owing to their low Tammann temperature and high surface energies, Au nanoparticles (NPs) are thermodynamically unstable and tend to minimize their surface energies by forming larger particles when exposed to elevated temperatures or upon prolonged storage. A concomitant loss of activity is observed following such ripening processes,[18−21] making the control of Au particle size, suitable selection of support materials, and engineering of the architecture of the metal–support interaction a significant challenge for catalyst preparation.[22−25] The efficient stabilization of Au NPs on support materials is therefore crucial for the development of Au nanocatalysts.

Several strategies aimed at stabilizing Au NPs for high-temperature oxidation processes have been established, such as the premodification of supports before Au NP loading,[26] the nanoconfinement of Au NPs within porous channels,[27,28] the creation of a strong metal–support interaction (SMSI) between

Received: October 6, 2016
Published: November 22, 2016

DOI: 10.1021/jacs.6b10472
J. Am. Chem. Soc. 2016, 138, 16130−16139

Scheme 1. Illustration Depicting the Construction of a Dopamine-Derived Layer Architecture for the Annealing Engineering of Au Nanocatalysts with High Thermal Stability

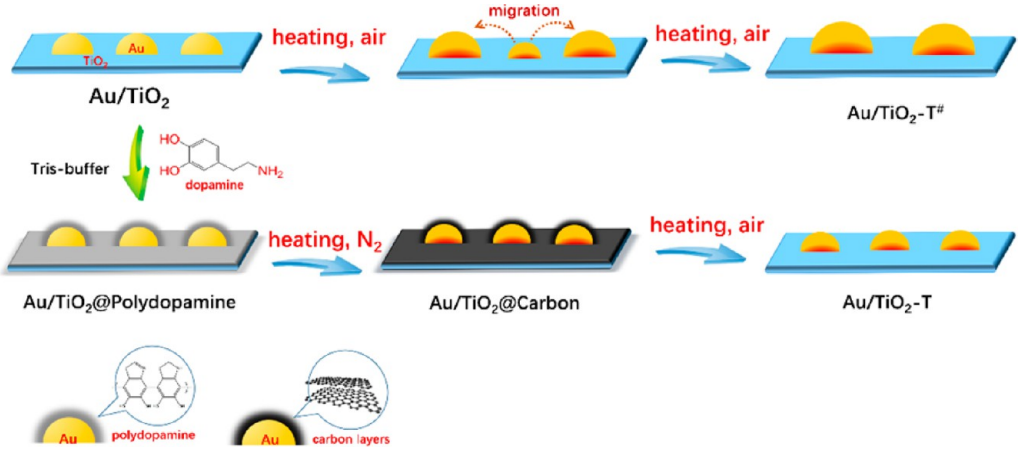

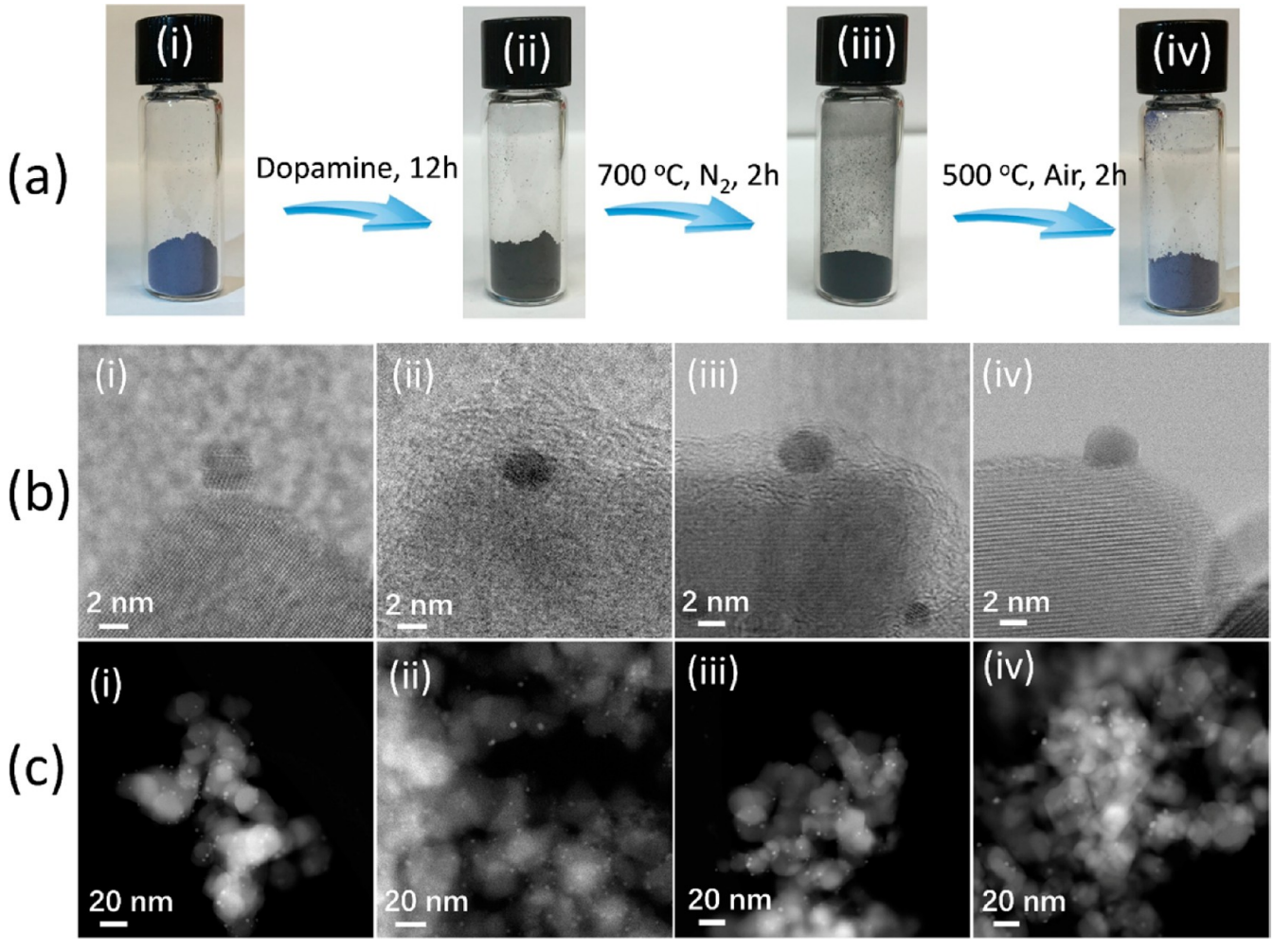

Figure 1. Photographs and nanomorphologies of Au nanocatalysts during each synthetic step. (a) Photographs; (b) BF-STEM and (c) HAADF-STEM images. (i) Au/TiO_2, (ii) Au/TiO_2@Polydopamine, (iii) Au/TiO_2@Carbon, and (iv) Au/TiO_2-500.

Au NPs and supports by substrate coatings,[29−31] and the encapsulation of Au NPs in core−shell or yolk−shell structures.[32,33] Even though significant progress has been achieved through these approaches, some issues remain to be addressed. For example, the Ostwald ripening process and the Brownian-like motion of Au cannot be well suppressed by premodification and nanoconfinement, and they still lead to the growth and coalescence of Au NPs.[26,34] With regard to the SMSI approach[29−31] and the encapsulation strategy,[24] although substrate coatings or inorganic shells can stabilize Au NPs well against sintering at elevated temperatures, they also reduce the activity of the catalyst by blocking active sites and/or causing diffusion limitations.[24] Re-exposing the active sites requires additional steps performed under harsh conditions to remove

DOI: 10.1021/jacs.6b10472
J. Am. Chem. Soc. 2016, 138, 16130−16139

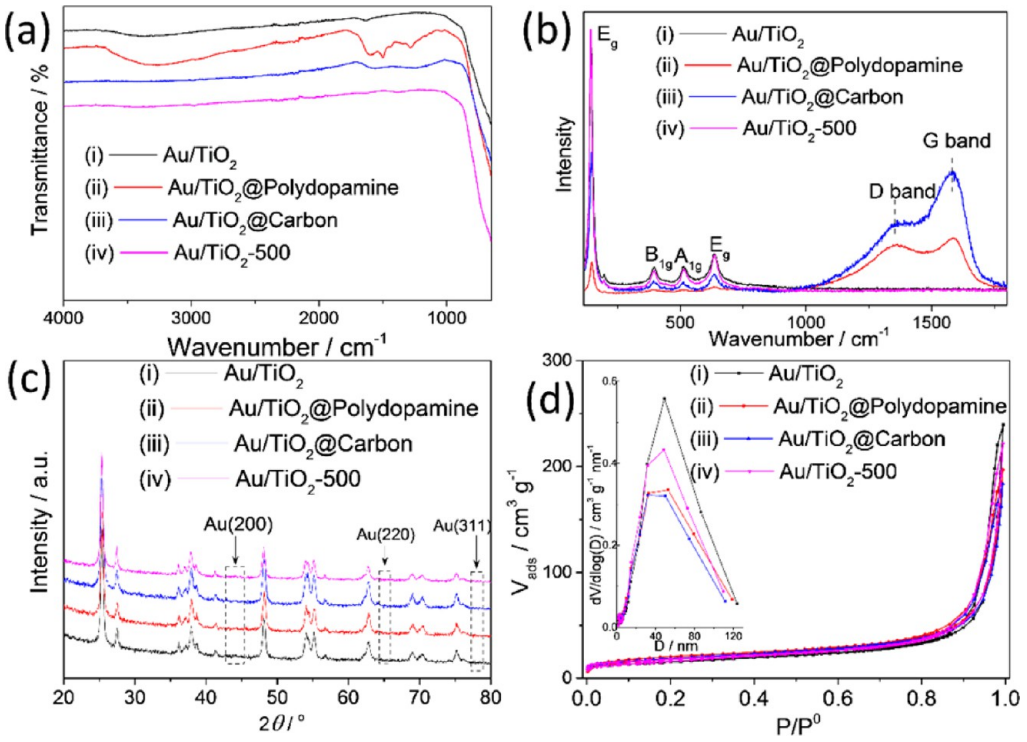

Figure 2. Structural characterization of Au nanocatalysts during each synthetic step. (a) FT-IR spectra; (b) Raman spectra; (c) XRD patterns; and (d) N_2-sorption isotherms and corresponding pore size distribution plots (inset).

coating layers. These steps involve the use of hazardous agents, resulting in the irreversible destruction of metal−support interfaces with accompanying reductions in stability.[35] Therefore, the development of a general synthetic strategy capable of stabilizing Au NPs on a broad range of supports without invoking SMSI or encapsulation is highly desirable.

Dopamine, which has a molecular structure similar to that of the adhesive proteins found in mussels, can form thin polydopamine films that adhere to virtually all surfaces, from nanoparticles to bulk materials.[36] Chemically, this coating process is a typical pH-induced polymerization that occurs quickly in a tris buffer solution (pH 8.5) at room temperature (25 °C).[36,37] Owing to this versatile coating chemistry that occurs under mild conditions, dopamine displays vast potential as a bioinspired building block for the construction of coating layers on supported Au NPs to stabilize them against sintering.

As illustrated in Scheme 1, dopamine molecules readily self-assemble on an Au nanocatalysts forming polydopamine layers with tunable thickness. Such a behavior is independent of the support in use, allowing exceptional versatility among diverse catalyst systems. Furthermore, unlike other protocols used to create coating layers, such as high-temperature hydrothermal treatment performed at 180−220 °C,[38] our dopamine self-assembly strategy utilizes much gentler reaction conditions and facilitates the preservation of small Au particle size.[39] Additionally, performing the self-assembly process in solution enables favorable mass transport and affords a conformal coating on the entire catalyst surface (both Au NPs and support), completely encapsulating the Au NPs within the polydopamine film.[37,39] This is a very important consideration, as complete encapsulation is one of the necessary steps in successful Au NP stabilization.

Following thermal annealing under an inert atmosphere, the polydopamine assemblies form rigid carbon shells covering the Au NPs, isolating them and preventing coalescence.[37] Annealing at elevated temperatures is also known to enhance contact between metal NPs and their supports via strong interfacial bonding, since metal NPs rearrange their atomic structures under high temperatures and form strong interactions with the surface defects on the support.[40−44] As a result of this structural rearrangement, the Au NPs become more energetically stable and thus retard the thermodynamically driven Ostwald ripening process.[45] As a result, the rate of NP sintering should be suppressed even after the removal of the carbon coatings.[40−45] In contrast, unencapsulated Au NPs can simultaneously undergo thermally induced sintering, resulting in larger domain formation, reduced surface area, and diminished catalytic performance.[24] Besides enabling stability improvements through thermal engineering, these artificial carbon shells are also beneficial for the long-term storage of Au nanocatalysts.[18]

The carbon shells covering the Au NPs can be removed easily, either by *in situ* activation under oxidative reaction conditions or through post-thermal treatment in air, stabilizing the Au NPs without destroying the well-established metal−support interfaces. Therefore, Au nanocatalyst systems improved by the treatment are expected to be resistant to sintering under oxidative reaction conditions. Detailed synthetic steps for the preparation and improvement of Au/TiO_2, a representative supported catalyst system, are provided in the Methods section.

RESULTS AND DISCUSSION

In Figure 1, the evolution of the microscopic structure of Au nanocatalysts during each synthesis step is seen in bright-field scanning transmission electron microscopy (BF-STEM) and aberration-corrected high-angle annular dark-field scanning transmission electron microscopy (HAADF-STEM) images.[46]

DOI: 10.1021/jacs.6b10472
J. Am. Chem. Soc. 2016, 138, 16130−16139

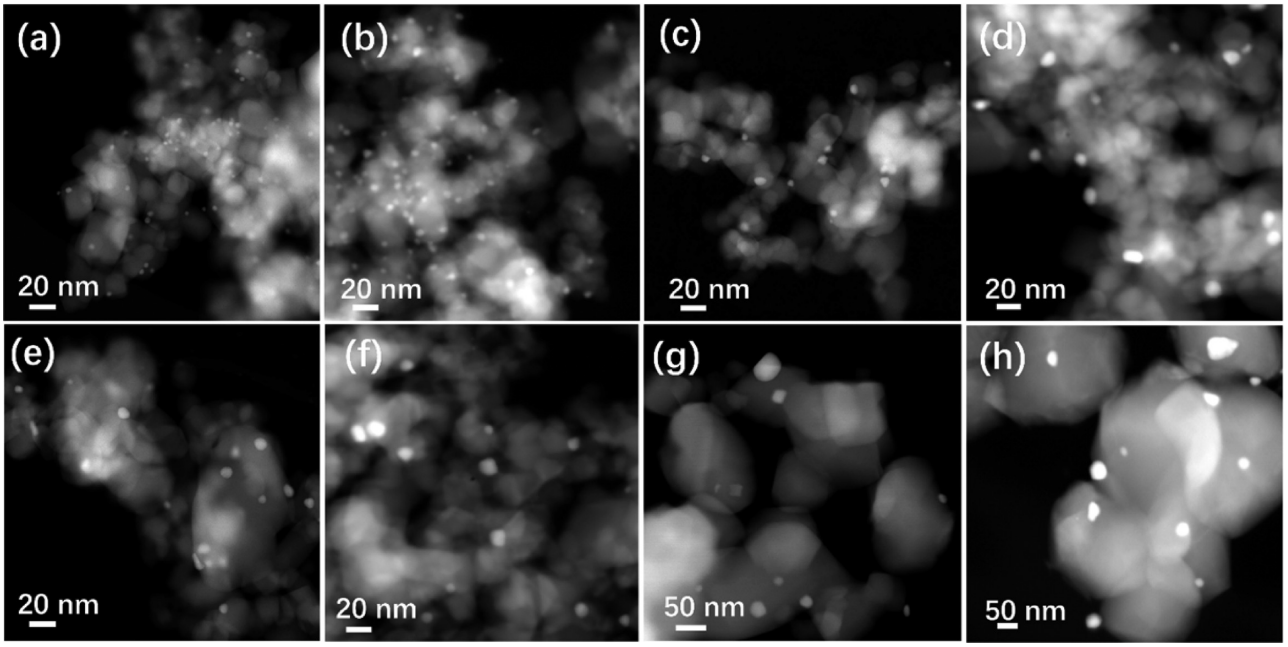

Figure 3. HAADF-STEM images of Au nanocatalysts annealed at temperatures ranging from 500 to 800 °C. (a) Au/TiO_2-500; (b) Au/TiO_2-600; (c) Au/TiO_2-700; (d) Au/TiO_2-800; (e) Au/TiO_2-500$^{\#}$; (f) Au/TiO_2-600$^{\#}$; (g) Au/TiO_2-700$^{\#}$; and (h) Au/TiO_2-800$^{\#}$.

For as-prepared Au/TiO_2, Au NPs with a size distribution of 3.0 ± 0.6 nm were homogeneously supported on TiO_2 crystallites with grain sizes of 20−60 nm (Figures 1b-I and S1). After 12 h of stirring in a tris buffer solution containing dopamine (denoted as Au/TiO_2@Polydopamine), both Au NPs and TiO_2 crystallites were completely covered by polydopamine assemblies without any growth in the particle size, underlining the advantage of a dopamine-based synthetic strategy for constructing shell architectures on Au nanocatalysts (Figure 1b-ii and Figure S2). Correspondingly, the sample color changed to dark brown, owing to the presence of the polydopamine layers (Figure 1a-i,ii).

After being subjected to thermal treatment at 700 °C in an N_2 flow for 2 h (denoted as Au/TiO_2@Carbon), the loose polymer layers transformed *in situ* to form carbon shells, which conformably covered the catalyst (Figures 1b-iii and S3). According to thermogravimetric analysis (TGA), Au/TiO_2@Carbon was determined to be 5.5 wt % carbon, which could be completely combusted in air below a temperature of 450 °C (Figure S4). Note that both Au NPs and TiO_2 NPs were well-protected against sintering even after harsh treatment at 700 °C (Figures 1 and S1), clearly underlining the unique structural benefits of the dopamine-derived shell architecture for stabilizing the Au nanocatalyst.[37,39] After postheating in air at 500 °C for 2 h, the carbon layers coating the Au/TiO_2 were completely removed, accompanied by a dramatic color change in the sample back to fuchsia. In comparison, the directly heated sample, Au/TiO_2-500$^{\#}$, was a deep blue color owing to the sintering of the Au NPs (Figure S5). The particle size of the resulting Au NPs was determined to be 3.8 ± 0.8 nm and 7.2 ± 1.4 nm for Au/TiO_2-500 and Au/TiO_2-500$^{\#}$, respectively (Figure S6). This result clearly demonstrates that the strategy of thermally annealing Au NPs enclosed within polydopamine-formed carbon shells was successful in stabilizing an Au nanocatalyst.[41,42,46]

The surface properties, crystallinity, specific surface area, and textural structure of the Au nanocatalyst were also investigated during each of the synthetic steps. Typical Fourier-transformed infrared (FT-IR) absorptions of polydopamine at 3650−3200 cm^{-1} (the stretching vibration of phenolic O−H and N−H), 1595 cm^{-1} (stretching vibration of aromatic ring and bending vibration of N−H), 1500 cm^{-1} (N−H shearing vibration), and 1340 cm^{-1} (stretching vibration of a CNC ring) were observed on Au/TiO_2@Polydopamine, demonstrating that polydopamine had successfully assembled on the Au nanocatalysts (plot ii in Figure 2a).[47] Correspondingly, two pronounced peaks assigned to the stretching and deformation of aromatic rings of polydopamine were also found in the Raman spectra (plot ii in Figure 2b).[47] The thermal transformation of polymer assemblies into carbon shells resulted in significant suppression of organic signatures in the FT-IR spectra, accompanied by the appearance of characteristic G- and D-bands of carbon species at 1580 and 1355 cm^{-1} in the Raman spectra (plot iii in Figure 2a,b). The intensity ratio of the G-band/D-band was determined to be 1.93, indicative of amorphous carbon layers.[48] After annealing in air at 500 °C for 2 h, the signals originating from the carbon species quickly disappeared in both the FT-IR and Raman spectra (plot iv in Figure 2a,b). This result is in good agreement with the observation of STEM images (Figure 1) and the analysis of *in situ* diffuse reflectance infrared Fourier transform spectroscopy (DRIFTS) of CO adsorption (Figure S7) and UV−vis diffuse reflectance spectra (Figure S8), which clearly indicate that the carbon layer coating on the catalyst had been completely removed. In addition, evident quenching of the stretching vibrations of surface-bonded hydroxyl groups and/or H_2O molecules at 3600−2800 and 1630 cm^{-1} in the FT-IR spectra was discovered in Au/TiO_2-500 (Figure S9).[49] These spectroscopic results indicate the surface properties of the TiO_2 support significantly changed following thermal annealing, which would influence the catalytic performance of the Au nanocatalyst in surface-sensitive reactions such as CO oxidation.[50]

Figure 2b,c shows the crystal structure of the TiO_2 support characterized by Raman spectra and X-ray diffraction (XRD)

DOI: 10.1021/jacs.6b10472
J. Am. Chem. Soc. 2016, 138, 16130−16139

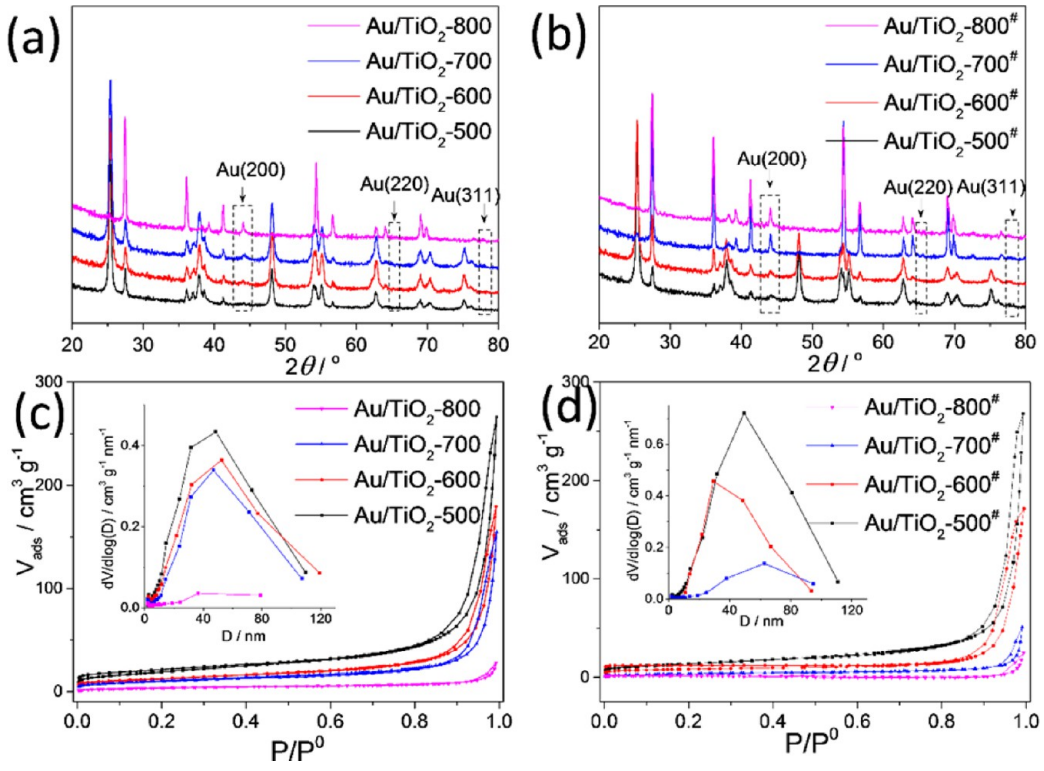

Figure 4. Structural characterization of Au nanocatalysts annealed at temperatures ranging from 500 to 800 °C. (a) XRD patterns and (c) N_2-sorption isotherms of Au/TiO_2-*T* series; (b) XRD patterns and (d) N_2-sorption isotherms. Insets in panels c and d are the pore size distribution plots.

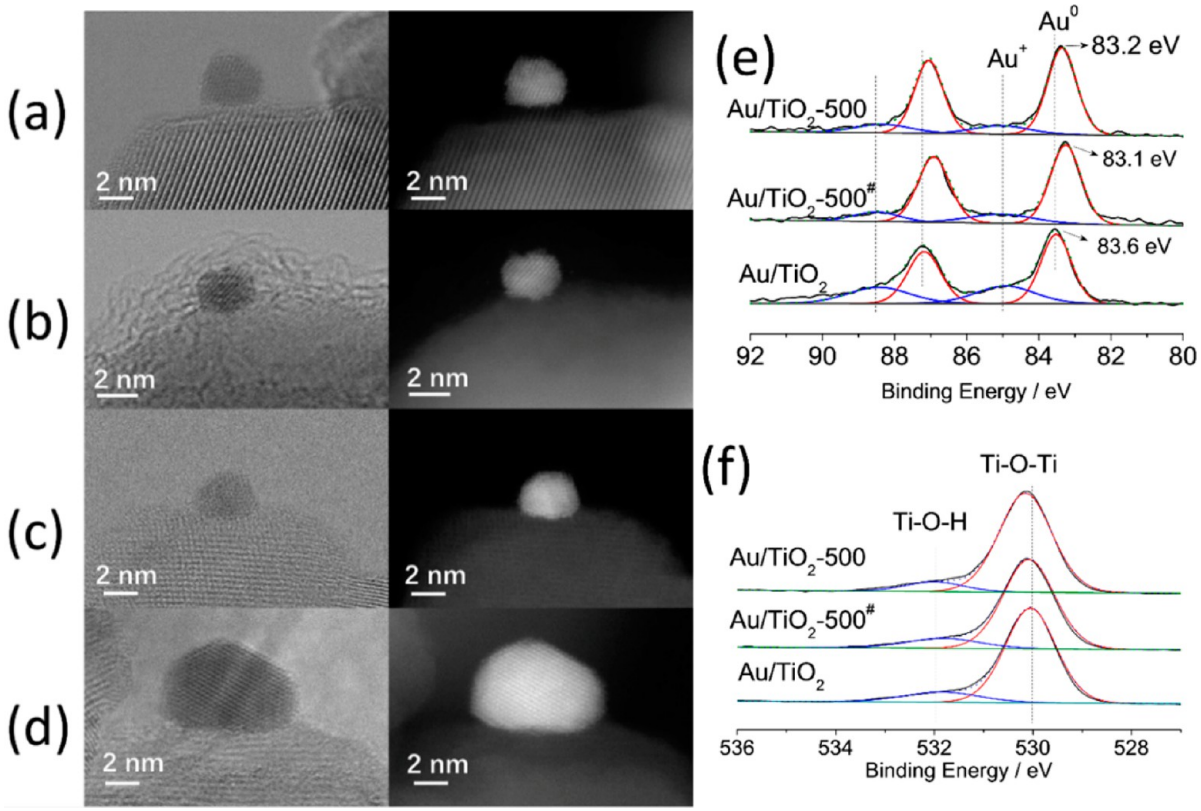

Figure 5. BF-STEM and HAADF-STEM images of (a) Au/TiO_2, (b) Au/TiO_2@Carbon, (c) Au/TiO_2-500, and (d) Au/TiO_2-500#, respectively. (e) Au 4f and (f) O 1s XPS spectra of Au/TiO_2, Au/TiO_2-500, and Au/TiO_2-500#.

DOI: 10.1021/jacs.6b10472
J. Am. Chem. Soc. 2016, 138, 16130−16139

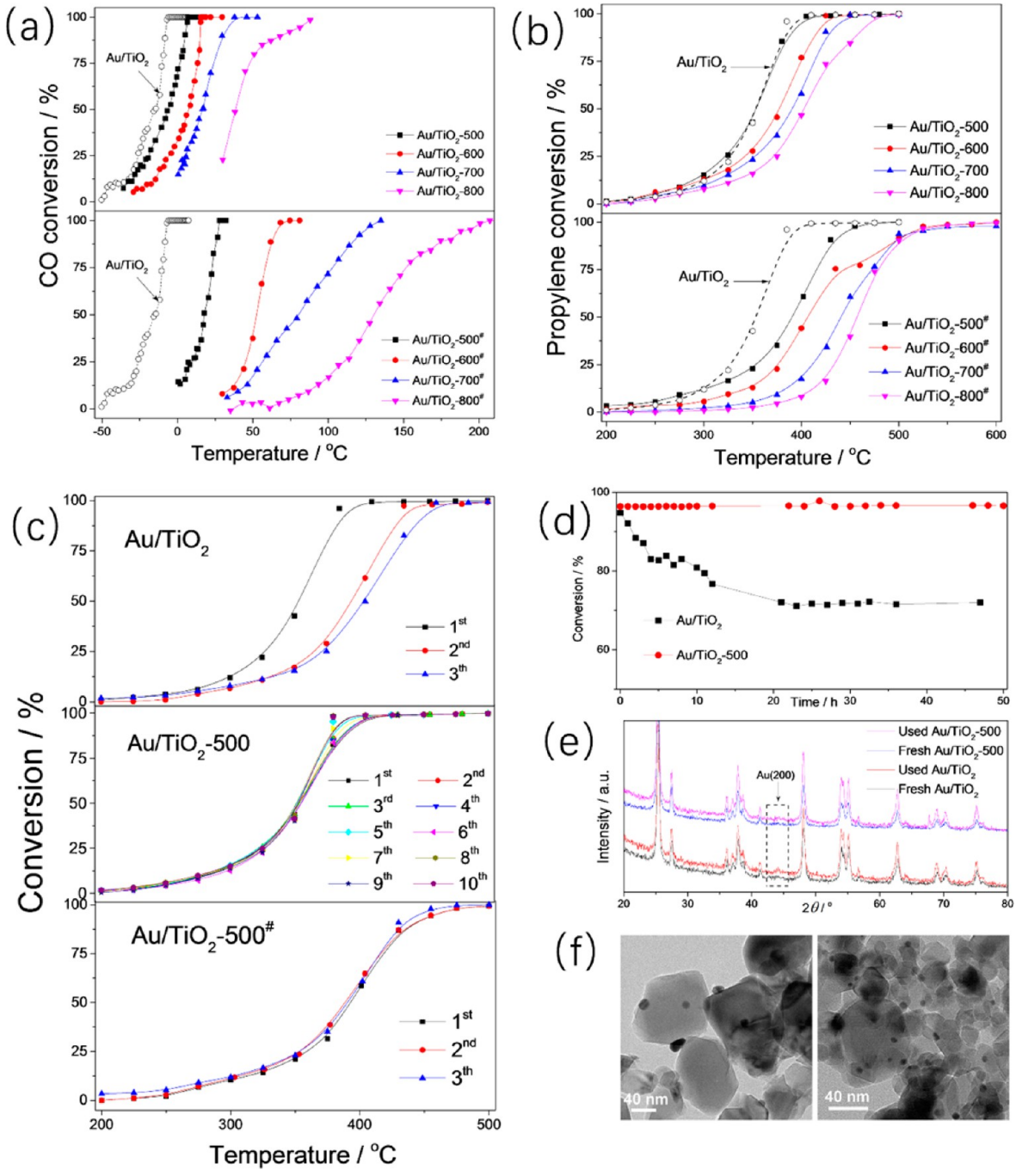

Figure 6. (a) CO and (b) propylene conversion vs reactor temperature on Au/TiO_2, Au/TiO_2-*T*, and Au/TiO_2-$T^{\#}$. (c) Repeating ignition−extinction cycles of propylene conversion on Au/TiO_2, Au/TiO_2-500, and Au/TiO_2-$500^{\#}$. (d) Long-term stability of propylene conversion on Au/TiO_2 and Au/TiO_2-500 at 400 °C. (e) XRD patterns of Au/TiO_2 and Au/TiO_2-500 before and after long-term reaction. (f) TEM images of Au/TiO_2 (left) and Au/TiO_2-500 (right) after long-term reaction.

patterns. Anatase was confirmed as the predominant phase without significant phase conversion,[51] owing to the complete coating of the entire catalyst surface by the carbon shells. No distinct diffraction peaks attributable to Au nanoparticles, such as Au (200) at 44°, Au (220) at 65°, or Au (311) at 78°, could be observed during any synthetic step. This observation confirmed the Au NPs were stabilized below 5 nm with uniform dispersion and was in good agreement with observations made by BF-STEM and HAADF-STEM.[33]

N_2-sorption isotherms, displayed in Figure 2d, reveal the textural structure of the Au nanocatalyst was also maintained by the dopamine-derived coatings. The slight decrease in the Barrett−Joyner−Halenda (BJH) pore size distribution of Au/TiO_2@Polydopamine and Au/TiO_2@Carbon can be attributed to the thin film assembly on the surfaces of the particles to reduce accumulated pores (Figure 2d, inset). Taken cumulatively, these characterizations conclusively demonstrate that polydopamine-derived carbon shells inhibit Au NP sintering and is a promising strategy for the engineering of supported Au nanocatalysts with improved thermal stability.[24]

To better evaluate the sintering resistance imparted by the polydopamine shell, a series of supported Au nanocatalysts

DOI: 10.1021/jacs.6b10472
J. Am. Chem. Soc. 2016, 138, 16130−16139

were annealed in air at temperatures ranging from 500 to 800 °C.[26] The resulting samples were denoted as Au/TiO_2-*T* and Au/TiO_2-$T^{\#}$, where # denotes the absence of dopamine coating and *T* indicates the annealing temperature (*T* = 500, 600, 700, and 800 °C). For the Au/TiO_2-*T* series, the thermally induced sintering of Au NPs was efficiently suppressed, even beyond the traditional annealing temperature (800 vs 700 °C). In contrast, the growth of Au NPs into larger particles with a relatively wide size distribution was clearly evident upon direct heating Au/TiO_2-$T^{\#}$. This has previously been attributed to insufficient interfacial bonding to stabilize Au (Figures 3 e–h and S6)[41,42,46] and clearly demonstrates the improvement imparted by our polydopamine encapsulation approach. In addition, careful examination revealed that not only the Au NPs but also the TiO_2 support were well protected from sintering after dopamine modification.

In Figure 4, the size evolution of Au NPs as a function of annealing temperature is investigated by the intensity of the Au (200) peak in XRD patterns. For Au/TiO_2-*T*, this characteristic peak emerged only when the temperature exceeded 600 °C and gradually increased with increasing annealing temperate. In contrast, for the Au/TiO_2-$T^{\#}$ series, the Au (200) peak is clearly visible on the 500 °C annealed sample, becoming much sharper and more pronounced with increasing temperature.[33] The thermally induced phase conversion of TiO_2 from anatase to rutile was also delayed on the Au/TiO_2-*T* samples (Figure 4a,b), affording a robust support for catalysis (Figure 4c,d). Thus, the introduction of polydopamine-derived carbon layers on Au/TiO_2 suppressed crystallite growth in both the TiO_2 support and the supported Au NPs during annealing engineering and clearly improved the thermal stability of the supported catalyst system at elevated temperatures.

To understand the excellent thermal stability of the Au/TiO_2-*T* series, BF-STEM images and corresponding aberration-corrected HAADF-STEM images were collected on randomly selected single Au NPs to investigate the metal–support interaction. For pristine Au/TiO_2, relatively modest contact between the Au NPs and the TiO_2 substrate was clearly observed, revealing insufficient interaction between the two (Figures 5a and S10).[46] As discussed previously, this is an important reason why supported Au NPs are so easily sintered.[16] However, after thermal annealing at 700 °C to rearrange the atomic structures within the carbon shell architecture, Au NPs with unchanged particle sizes were strongly anchored onto the underlying TiO_2 via interfacial bonding with the oxygen vacancies (Figured 5b and S11).[46] During a 500 °C annealing in air to remove carbons, such intimate contact could generate sufficient interaction to efficiently suppress the migration and aggregation of Au NPs, greatly improving their thermal stability (Figured 5c and S12).[41,42] Improved interfacial contact between Au NPs and TiO_2 was also observed in Au/TiO_2-500$^{\#}$, but irreversible growth of the Au NPs also occurred during the thermal annealing because of the lack of a carbon shell (Figures 5d and S13).

Figure 5e,f shows the results of X-ray photoelectron spectroscopy (XPS) conducted to characterize the metal–support interaction. In the Au 4f XPS spectra, the binding energy of Au $4f_{7/2}$ was determined to be 83.6 eV for Au/TiO_2, in good agreement with literature data for metallic gold.[52] After thermal annealing at 500 °C for 2 h, an obvious shift of binding energy to 83.2 eV (Au/TiO_2-500) and 83.1 eV (Au/TiO_2-500$^{\#}$) was observed, indicating the Au NPs supported on TiO_2 had become electron-rich.[42,52] This finding was further confirmed by the *in situ* DRIFT spectra of CO adsorption, in which the negatively charged Au enhanced CO absorption at 2075 cm^{-1} (Figure S7). According to previous reports,[42,46,52] the electron transfer from the support (perhaps from the oxygen vacancies) to metal NPs is a strong indicator of the improved interfacial contact between Au NPs and TiO_2, which is consistent with the observed fast quenching of photoluminescence spectra (Figure S14). As a consequence of this electron transfer, the atomic ratio of cationic Au decreased significantly from 33.2% to 15.5 and 19.5% for Au/TiO_2-500 and Au/TiO_2-500$^{\#}$, respectively. In the O 1s XPS spectra, the primary peak at around 530 eV and the shoulder peak at 532.0 eV were attributed to the oxygen species contained in Ti–O–Ti and Ti–O–H.[52] As a result of annealing at high temperature, the primary peak shifted slightly toward a higher binding energy; more importantly, the Ti–O–H species decreased from 20.1 to 14.0 atom % for Au/TiO_2-500, and to 15.2 atom % for Au/TiO_2-500$^{\#}$, in good agreement with the FT-IR results showing the elimination of surface-bonded hydroxyl groups. In the Ti 2p spectra (Figure S15), no difference in titanium species was discovered among the three samples, indicating their similar electronic properties. Thus, a strong electronic interaction between Au NPs and TiO_2 had been created via annealing engineering to improve their interfacial contact, leading to electron-rich Au.

CO oxidation is a simple but typical probe reaction for the fundamental study of Au nanocatalysts to increase understanding of their catalytic properties, particularly size-dependent behavior.[53] For that reason, the Au nanocatalysts were subjected to CO oxidation. Figure 6a shows the CO oxidation achieved on Au nanocatalysts was strongly dependent on the particle size of the supported Au NPs. With respect to their smaller particle sizes, the Au/TiO_2-*T* samples exhibited much higher activity compared with their Au/TiO_2-$T^{\#}$ counterparts, clearly revealing the strong size dependence on catalytic performance. In addition, the well-preserved crystal structure and nanotexture of TiO_2 contributed to the superior catalytic performance in CO oxidation of Au/TiO_2-*T* samples, colloquially known as the support effect. According to the light-off conversion curves, the temperatures required for 50% CO conversion (T_{50}) were determined to be −7, 6, 16, and 39 °C for Au/TiO_2-*T* (*T* = 500, 600, 700, and 800 °C), much lower than the T_{50} of 17, 52, 79, and 130 °C for Au/TiO_2-$T^{\#}$ (*T* = 500, 600, 700, and 800 °C), clearly revealing size-dependent catalytic behavior. Note that the difference in catalytic activity between Au/TiO_2 and Au/TiO_2-500 is mainly attributable to the elimination of surface-bonded hydroxyl groups on the support, rather than the slight growth of the Au NPs (3.0 ± 0.6 nm vs 3.8 ± 0.8 nm, Figure S1), since hydroxyl groups can react with CO through a smaller barrier, compared to that of the reaction CO + O →CO_2.[50,54] The evolution of the crystalline and textural structure of the TiO_2 support can be also excluded as a reason for the decrease in catalytic performance, owing to their comparable XRD patterns and N_2-sorption isotherms. To further eliminate the influence of size effects on catalytic performance, TiO_2 with and without abundant hydroxyl groups was selected as the support for the colloidal Au NP (ca. 6 nm) dispersion (Figure S16). In Figure S16b, a higher activity for CO conversion is evident on the hydroxyl group rich Au/TiO_2 nanocatalyst, exhibiting a strong support effect for CO oxidation. For the kinetic study of CO oxidation on Au/TiO_2 nanocatalysts, the reaction rates and turnover number (TOF)

DOI: 10.1021/jacs.6b10472
J. Am. Chem. Soc. 2016, 138, 16130–16139

were collected and compared with the reported results in Table S1.

To better evaluate the catalytic durability against thermal sintering, the catalytic combustion of propylene at elevated temperatures (e.g., 400 °C) was chosen as a high-temperature reaction model, rather than the CO oxidation, in which Au nanocatalysts exhibit stable behaviors at temperatures no more than 50 °C (Figure S17). In Figure 6b, similar size-dependent activity was observed for the Au nanocatalyst in propylene oxidation, during which the Au/TiO_2-T samples still exhibited much higher activity than the Au/TiO_2-$T^{\#}$ series. The T_{50} of propylene conversion was determined to be 352, 376, 391, and 403 °C for Au/TiO_2-T (T = 500, 600, 700, and 800 °C) and 390, 406, 441, and 458 °C for Au/TiO_2-$T^{\#}$ (T = 500, 600, 700, and 800 °C), clearly correlated to the sizes of the Au NPs. The high-temperature catalytic stability was examined by successive ignition−extinction cycles; the results are shown in Figures 6c and S18. For Au/TiO_2, a significant loss of activity toward a much higher T_{50} occurred immediately in the second run, presumably because the metal−support interaction was insufficient to stabilize the Au NPs against sintering.[41,42] In contrast, robust activity without any loss in T_{50} was obtained on both Au/TiO_2-T and Au/TiO_2-$T^{\#}$ even after 10 ignition−extinction cycles. This finding conclusively demonstrates that annealing at elevated temperatures indeed can suppress secondary crystallite growth during catalysis, affording ultrastable supported Au nanocatalysts.[41,42,46]

Compared with those of Au/TiO_2-$T^{\#}$, the higher activities obtained on Au/TiO_2-T are a good example displaying the importance of the core−shell nanostructure in stabilizing Au NPs during high-temperature annealing. To underline the necessity of stabilization through high-temperature annealing,[42] a reference sample was synthesized by direct heating of Au/TiO_2@Polydopmine in air at 500 °C for 2 h (denoted as Au/TiO_2-500*). As shown in Figure S19, significantly decreased activity was observed on Au/TiO_2-500*, clearly indicating the inevitable sintering of the Au NPs occurred without high-temperature annealing (Au/TiO_2-500* vs Au/TiO_2-500). Nevertheless, the activity of Au/TiO_2-500* was still higher than that of Au/TiO_2-500$^{\#}$, presumably because the polydopamine layers can partially slow Au NP growth during annealing under air.

Figure 6d displays data for Au/TiO_2-500 after 10 repeated ignition−extinction cycles followed by a long period of operation at 400 °C. Fresh Au/TiO_2 is displayed as a reference. The initial propylene conversion ratio obtained on the recycled Au/TiO_2-500 was ∼96%, comparable to that of fresh Au/TiO_2. This finding demonstrates that the Au NPs were stabilized against sintering even after 10 successive runs. Furthermore, there was no deactivation of the recycled Au/TiO_2-500 when the catalytic reaction was performed at 400 °C for 50 h, demonstrating its robust sintering-resistant catalytic performance. In contrast, the fresh Au/TiO_2 displayed a rapid drop in conversion ratio from 96 to 70% over the initial 23 h as a result of the significant growth of the Au NPs into larger particles (Figure 6e,f). The activity subsequently stabilized following the creation of enhanced bonding between the Au and TiO_2, immobilizing the Au NPs and preventing secondary growth. Both Au/TiO_2 and Au/TiO_2-500 were investigated by XRD (Figure 6e), transmission electron microscopy (TEM, Figure 6f), HR-TEM (Figure S20c,d), and FT-IR after long-term operation. Significant sintering of the Au NPs is clearly observable on the used Au/TiO_2, with the rise of a pronounced Au (200) peak in the XRD pattern and significant growth of the Au NPs, to up to 15 nm, apparent in the TEM image. These results are quite different from the observation of the used Au/TiO_2-500, the particle size of which remained around 4 nm, and are without a detectable Au (200) reflection.[55,56]

CONCLUSIONS

A general synthetic strategy aimed at stabilizing Au NPs on a broad range of supports under high-temperature oxidation processes was successfully developed. Owing to the structural rigidity and thermal stability of the resulting carbonaceous materials, the dopamine-derived carbon shells that form a conformal coating on catalysts can efficiently isolate Au NPs and prevent sintering during annealing, strengthening the metal−support bonding. This thermally induced enhancement in interfacial bonding can efficiently stabilize Au NPs against secondary crystallite growth during high-temperature oxidation processes, even after removal of the carbon shells, resulting in a robust sintering-resistant Au nanocatalyst for catalytic combustion of propylene at elevated temperatures. It is interesting that the resulting Au nanocatalyst is also very stable under a reducing environment at elevated temperatures (Figure S21), which is also beneficial for its practical applications. Further study focused on investigating the metal−support interaction is ongoing to support the design and synthesis of ultrastable Au nanocatalysts. Furthermore, it is expected that the current synthetic strategy can be extended to stabilizing other supported catalysts, such as platinum (Figure S22) and palladium (Figure S23), using dopamine-derived carbon architectures to prevent sintering during annealing treatment.

METHODS

Synthesis of Au/TiO_2. Au/TiO_2 was prepared by the deposition−precipitation method. Typically, a solution containing 0.02 g of $HAuCl_4$·3H2O in water (60 mL) was adjusted to pH 10.0 using 1 M NaOH. After heating at 70 °C, 1 g of TiO_2 (Degussa P25) was added, and the slurry was magnetically stirred for 2 h. The suspension was separated by centrifugation and washed with deionized water until free of chloride ions. The product was dried at 40 °C under vacuum and then calcined at 250 °C in air for 2 h. Before use, the resulting sample was kept at room temperature in a desiccator connected to the vacuum. The Au content was determined to be 1.08 wt % by inductively coupled plasma-optical emission spectrometry (ICP-OES).

Synthesis of Au/TiO_2-T. First, 0.5 g of as-prepared Au/TiO_2 was stirred in dopamine-containing (1 mg mL^{-1}) tris-buffer solution (100 mL, 10 mM; pH 8.5) for 24 h. The suspension was separated by centrifugation, washed with deionized water three times and ethanol one time, and then dried at 40 °C under vacuum. The obtained sample was denoted as Au/TiO_2@Polydopamine and was subjected to annealing treatment at 700 °C in N_2 flow for 2 h at a heating rate of 5 °C min^{-1}. The resulting sample was denoted as Au/TiO_2@Carbon. Then, the Au/TiO_2-T series were synthesized by directly heating Au/TiO_2@Carbon in air at different temperatures for 2 h at a heating rate of 5 °C min^{-1}, where T (500, 600, 700, and 800) is representative of the heating temperature (°C).

Synthesis of Au/TiO_2-$T^{\#}$. The Au/TiO_2-$T^{\#}$ series were synthesized by directly heating Au/TiO_2 in air at different temperatures for 2 h with a heating rate of 5 °C min^{-1}, where T (500, 600, 700, and 800) is representative of the heating temperature (°C).

Synthesis of Au/TiO_2-500*. Au/TiO_2-500* was synthesized by directly heating Au/TiO_2@Polydopamine in air at 500 °C for 2 h at a heating rate of 5 °C min^{-1}.

Characterization of Prepared Au/TiO_2 Catalysts. The gold content of the catalysts was determined by inductively coupled-plasma atomic emission spectroscopy (ICP-AES) using a PerkinElmer Optima 2100 DV spectrometer. X-ray diffraction (XRD) measurements were

DOI: 10.1021/jacs.6b10472
J. Am. Chem. Soc. 2016, 138, 16130−16139

carried out on a PANalytical X'Pert Pro MPD diffractometer using an X'Celerator RTMS detector. Scanning transmission electron microscopy (STEM) analyses were carried out on a Hitachi HD2700C (200 kV) with a probe aberration corrector. Nitrogen adsorption−desorption isotherms were measured at −196 °C on an ASAP 2010 analyzer (Micromeritics Co. Ltd.). Before the measurement, the sample was degassed at 150 °C for 24 h under vacuum to remove moisture and impurities. The Brumauer−Emmett−Teller (BET) method was used to calculate the specific surface areas and pore sizes of samples. The FT-IR spectra of samples were recorded on a PerkinElmer Frontier FT-IR spectrometer. Thermogravimetric analysis (TGA) was performed on a TG209 (NETZSCH Co.). Raman spectroscopy was performed on a Renishaw Invia+Reflex Raman spectrometer with a CCD detector, and the wavelength of the excitation line was 514 nm. X-ray photoelectron spectroscopy (XPS) data were collected using a Thermo ESCALAB 250 spectrometer with a monochromatized Al Kα X-ray source (1486.6 eV) and an applied power of 150 W. Ti $2p_{3/2}$ (binding energy 458.8 eV) was used as the reference.

Catalytic Activity Measurement. The catalytic activity of Au/TiO_2 catalysts for both CO oxidation and propene combustion was evaluated. CO oxidation was carried out in a temperature-controlled microreactor (Altamira AMI 200) equipped with an online gas chromatograph. A gaseous mixture of CO (1 vol %) balanced in dry air was passed through 30 mg of the catalyst at a total flow rate of 10 mL·min^{-1} (corresponding to a space velocity of 20,000 mL·g_{cat}^{-1}·h^{-1}). The inlet and outlet gas compositions were analyzed online by a gas chromatograph equipped with a thermal conductivity detector (TCD). CO conversion is the percentage of CO oxidized to CO_2 after the reaction.

Propene combustion was carried out in a fixed-bed flow reactor system. A 50 mg sample of catalyst was diluted in 500 mg of quartz powder. The feed gas was composed of 5 vol % propene, 25 vol % O_2, and 70 vol % N_2, and the total flow rate was 10 mL·min^{-1} (corresponding to a space velocity of 12 000 mL·g_{cat}^{-1}·h^{-1}). The inlet and outlet gas compositions were analyzed online by a gas chromatograph (FuLi GC9790) equipped a flame ionization detector (FID). Propene conversion is the percentage of propene reduction after the reaction.

■ ASSOCIATED CONTENT

Supporting Information

The Supporting Information is available free of charge on the ACS Publications website at DOI: 10.1021/jacs.6b10472.

CO oxidation rates, particle size distribution, TEM and STEM images, TGA curve, photographs of nanocatalysts, *in situ* DRIFTS results, UV−vis DRS, FT-IR spectra, BF- and HAADF-STEM images, PL spectra, XPS spectra, ignition−extinction cycles, and characterization data (PDF)

■ AUTHOR INFORMATION

Corresponding Authors

*jinshui.zhang@hotmail.com
*dais@ornl.gov

ORCID

Yanqin Wang: 0000-0002-5636-0617
Jinshui Zhang: 0000-0003-4649-6526
Sheng Dai: 0000-0002-8046-3931

Present Address

Q.H.: Cardiff Catalysis Institute and School of Chemistry, Cardiff University, Cardiff CF10 3AT, United Kingdom.

Notes

The authors declare no competing financial interest.

■ ACKNOWLEDGMENTS

W.C.Z., Y.L.G., and G.Z.L. appreciate the financial support from the National Key Basic Research Program of China (2013CB933200), the National Key Research and Development Program of China (2016YFC0204300), and 111 project (B08021). Y.G. appreciates the National Natural Science Foundation of China (21571061); J.Z. and S.D. were supported by the U.S. Department of Energy, Office of Science, Basic Energy Sciences, Chemical Sciences, Geosciences, and Biosciences Division. Q.H. and A.Y.B were supported by the U.S. Department of Energy, Office of Science, Basic Energy Sciences, Materials Sciences and Engineering Division, and through a user project supported by the Oak Ridge National Laboratory (ORNL) Center for Nanophase Materials Sciences, sponsored by the Scientific User Facilities Division, Office of Science, Basic Energy Sciences, U.S. Department of Energy. J.Z. and S.D. thank Dr. C. Abney (ORNL) for his helpful suggestions.

■ REFERENCES

(1) Hutchings, G. J. *J. Catal.* **1985**, *96*, 292.
(2) Haruta, M.; Kobayashi, T.; Sano, H.; Yamada, N. *Chem. Lett.* **1987**, *16*, 405.
(3) Haruta, M.; Daté, M. *Appl. Catal., A* **2001**, *222*, 427.
(4) Hashmi, A. S. K.; Hutchings, G. J. *Angew. Chem., Int. Ed.* **2006**, *45*, 7896.
(5) Haruta, M. *Nature* **2005**, *437*, 1098.
(6) Enache, D. I.; Edwards, J. K.; Landon, P.; Solsona-Espriu, B.; Carley, A. F.; Herzing, A. A.; Watanabe, M.; Kiely, C. J.; Knight, D. W.; Hutchings, G. J. *Science* **2006**, *311*, 362.
(7) Kesavan, L.; Tiruvalam, R.; Rahim, M. H. A.; bin Saiman, M. I.; Enache, D. I.; Jenkins, R. L.; Dimitratos, N.; Lopez-Sanchez, J. A.; Taylor, S. H.; Knight, D. W.; Kiely, C. J.; Hutchings, G. J. *Science* **2011**, *331*, 195.
(8) Villa, A.; Dimitratos, N.; Chan-Thaw, C.; Hammond, C.; Prati, L.; Hutchings, G. J. *Acc. Chem. Res.* **2015**, *48*, 1403.
(9) Gu, D.; Tseng, J.; Weidenthaler, C.; Bongard, H.; Spliethoff, B.; Schmidt, W.; Soulimani, F.; Weckhuysen, B.; Schüth, F. J. *J. Am. Chem. Soc.* **2016**, *138*, 9572.
(10) Thompson, D. T. *Gold Bull.* **2001**, *34*, 134.
(11) Chen, M. S.; Goodman, D. W. *Science* **2004**, *306*, 252.
(12) Schauermann, S.; Nilius, N.; Shaikhutdinov, S.; Freund, H.-J. *Acc. Chem. Res.* **2013**, *46*, 1673.
(13) Haruta, M. *Catal. Today* **1997**, *36*, 153.
(14) Majimel, J.; Lamirand-Majimel, M.; Moog, I.; Feral-Martin, C.; Tréguer-Delapierre, M. *J. Phys. Chem. C* **2009**, *113*, 9275.
(15) Prati, L.; Villa, A. *Acc. Chem. Res.* **2014**, *47*, 855.
(16) Yusuf, S.; Jiao, F. *ACS Catal.* **2012**, *2*, 2753.
(17) Bokhimi, X.; Zanella, R.; Morales, A. *J. Phys. Chem. C* **2007**, *111*, 15210.
(18) Wu, Y.; Sun, K.-Q.; Yu, J.; Xu, B.-Q. *Phys. Chem. Chem. Phys.* **2008**, *10*, 6399.
(19) Qiao, B.; Liang, J.-X.; Wang, A.; Xu, C.-Q.; Li, J.; Zhang, T.; Liu, J. J. *Nano Res.* **2015**, *8*, 2913.
(20) Han, C.; Majumdar, P.; Marinero, E.; Aguilar-Tapia, A.; Zanella, R.; Greeley, J.; Ortalan, V. *Nano Lett.* **2015**, *15*, 8141.
(21) Weiher, N.; Beesley, A.; Tsapatsaris, N.; Delannoy, L.; Louis, C.; van Bokhoven, J.; Schroeder, S. *J. Am. Chem. Soc.* **2007**, *129*, 2240.
(22) Chen, M.; Goodman, D. W. *Acc. Chem. Res.* **2006**, *39*, 739.
(23) Lamallem, M.; Cousin, R.; Thomas, R.; Siffert, S.; Aïssi, F.; Aboukaïs, A. *C. R. Chim.* **2009**, *12*, 772.
(24) Cao, A.; Lu, R.; Veser, G. *Phys. Chem. Chem. Phys.* **2010**, *12*, 13499.
(25) Lu, J.; Fu, B.; Kung, M.; Xiao, G.; Elam, J. W.; Kung, H.; Stair, P. C. *Science* **2012**, *335*, 1205.
(26) Yan, W.; Mahurin, S. M.; Pan, Z.; Overbury, S. H.; Dai, S. *J. Am. Chem. Soc.* **2005**, *127*, 10480.

DOI: 10.1021/jacs.6b10472
J. Am. Chem. Soc. 2016, 138, 16130−16139

(27) Laursen, A. B.; Højholt, K. T.; Lundegaard, L. F.; Simonsen, S. B.; Helveg, S.; Schüth, F.; Paul, M.; Grunwaldt, J.-D.; Kegnæs, S.; Christensen, C. H.; Egeblad, K. *Angew. Chem., Int. Ed.* **2010**, *49*, 3504.
(28) Wang, S.; Wang, J.; Zhu, X.; Wang, J.; Terasaki, O.; Wan, Y. *Chin. J. Catal.* **2016**, *37*, 61.
(29) Liu, X.; Liu, M.-H.; Luo, Y.-C.; Mou, C.-Y.; Lin, S. D.; Cheng, H.; Chen, J.-M.; Lee, J.-F.; Lin, T.-S. *J. Am. Chem. Soc.* **2012**, *134*, 10251.
(30) Tang, H.; Wei, J.; Liu, F.; Qiao, B.; Pan, X.; Li, L.; Liu, J.; Wang, J.; Zhang, T. *J. Am. Chem. Soc.* **2016**, *138*, 56.
(31) Tang, H.; Liu, F.; Wei, J.; Qiao, B.; Zhao, K.; Su, Y.; Jin, C.; Li, L.; Liu, J.; Wang, J.; Zhang, T. *Angew. Chem., Int. Ed.* **2016**, *55*, 10606.
(32) Lu, J.; Elam, J. W.; Stair, P. C. *Acc. Chem. Res.* **2013**, *46*, 1806.
(33) Ma, Z.; Brown, S.; Howe, J. Y.; Overbury, S. H.; Dai, S. *J. Phys. Chem. C* **2008**, *112*, 9448.
(34) Liu, Z.; Che, R.; Elzatahry, A. A.; Zhao, D. *ACS Nano* **2014**, *8*, 10455.
(35) Zhang, Y.; Zhou, Y.; Zhang, Z.; Xiang, S.; Sheng, X.; Zhou, S.; Wang, F. *Dalton Trans.* **2014**, *43*, 1360.
(36) Lee, H.; Dellatore, S. M.; Miller, W. M.; Messersmith, P. B. *Science* **2007**, *318*, 426.
(37) Liu, R.; Mahurin, S. M.; Li, C.; Unocic, R. R.; Idrobo, J. C.; Gao, H.; Pennycook, S. J.; Dai, S. *Angew. Chem., Int. Ed.* **2011**, *50*, 6799.
(38) Ji, T.; Li, L.; Wang, M.; Yang, Z.; Lu, X. *RSC Adv.* **2014**, *4*, 29591.
(39) Chung, D. Y.; Jun, S. W.; Yoon, G.; Kwon, S. G.; Shin, D. Y.; Seo, P.; Yoo, J. M.; Shin, H.; Chung, Y.-H.; Kim, H.; Mun, B. S.; Lee, K.-S.; Lee, N.-S.; Yoo, S. J.; Lim, D.-H.; Kang, K.; Sung, Y.-E.; Hyeon, T. *J. Am. Chem. Soc.* **2015**, *137*, 15478.
(40) Matthey, D.; Wang, J. G.; Wendt, S.; Matthiesen, J.; Schaub, R.; Lægsgaard, E.; Hammer, B.; Besenbacher, F. *Science* **2007**, *315*, 1692.
(41) Goodman, D. W. *Catal. Lett.* **2005**, *99*, 1.
(42) Tsubota, S.; Nakamura, T.; Tanaka, K.; Haruta, M. *Catal. Lett.* **1998**, *56*, 131.
(43) Bernal, S.; Calvino, J. J.; Cauqui, M. A.; Gatica, J. M.; Larese, C.; Pérez Omil, J. A.; Pintado, J. M. *Catal. Today* **1999**, *50*, 175.
(44) Kang, Y.; Ye, X.; Chen, J.; Qi, L.; Diaz, R. E.; Doan-Nguyen, V.; Xing, G.; Kagan, C. R.; Li, J.; Gorte, R. J.; Stach, E. A.; Murray, C. B. *J. Am. Chem. Soc.* **2013**, *135*, 1499.
(45) Ratke, L.; Voorhees, P. *Growth and Coarsening: Ostwald Ripening in Material Processing*; Springer: New York, 2002.
(46) Ta, N.; Liu, J.; Chenna, S.; Crozier, P. A.; Li, Y.; Chen, A.; Shen, W. *J. Am. Chem. Soc.* **2012**, *134*, 20585.
(47) Zheng, X.; Zhang, J.; Wang, J.; Qi, X.; Rosenholm, J. M.; Cai, K. *J. Phys. Chem. C* **2015**, *119*, 24512.
(48) Zhang, J.; Qiao, Z.-A.; Mahurin, S. M.; Jiang, X.; Chai, S.-H.; Lu, H.; Nelson, K.; Dai, S. *Angew. Chem., Int. Ed.* **2015**, *54*, 4582.
(49) Takeuchi, M.; Martra, G.; Coluccia, S.; Anpo, M. *J. Phys. Chem. B* **2005**, *109*, 7387.
(50) Davó-Quiñonero, A.; Navlani-García, M.; Lozano-Castelló, D.; Bueno-López, A.; Anderson, J. A. *ACS Catal.* **2016**, *6*, 1723.
(51) Nuño, M.; Ball, R. J.; Bowen, C. R.; Kurchania, R.; Sharma, G. D. *J. Mater. Sci.* **2015**, *50*, 4822.
(52) Wang, L.; Wang, H.; Rice, A. E.; Zhang, W.; Li, X.; Chen, M.; Meng, X.; Lewis, J. P.; Xiao, F.-S. *J. Phys. Chem. Lett.* **2015**, *6*, 2345.
(53) Guan, H.; Lin, J.; Qiao, B.; Yang, X.; Li, L.; Miao, S.; Liu, J.; Wang, A.; Wang, X.; Zhang, T. *Angew. Chem., Int. Ed.* **2016**, *55*, 2820.
(54) Wang, H.-F.; Kavanagh, R.; Guo, Y.-L.; Guo, Y.; Lu, G.-Z.; Hu, P. *Angew. Chem., Int. Ed.* **2012**, *51*, 6657.
(55) Hutchings, G.; Zhang, Y.; Li, J.; Yonemoto, B.; Zhou, X.; Zhu, K.; Jiao, F. *J. Am. Chem. Soc.* **2015**, *137*, 4223.
(56) Lu, Q.; Rosen, J.; Zhou, Y.; Hutchings, G. S.; Kimmel, Y. C.; Chen, J. G.; Jiao, F. *Nat. Commun.* **2014**, *5*, 3242.

DOI: 10.1021/jacs.6b10472
J. Am. Chem. Soc. 2016, 138, 16130−16139